HIP-HOP: Invariants for 2D Tilings with Biomedical Case Study

Madhava Gaikwad
Microsoft
mgaikwad@microsoft.com

Ashwini Doke
Department of Computer Science and Engineering
Amrita School of Computing, Amrita Vishwa Vidyapeetham, Bengaluru, India
bl.en.r4cse20004@bl.students.amrita.edu

Abstract

We present HIP-HOP, a pair of geometric invariants for two-dimensional cellular tilings. HOP captures orientational order among neighbors, while HOI quantifies polygonal regularity. Both are invariant to translation, rotation, and scale, and robust to segmentation noise and null models. Applied to corneal endothelium, HIP-HOP separates control and PMMA groups more consistently than standard morphometric indices. HIP-HOP thus serves as a clinically relevant descriptor and an interpretable benchmark for representation learning.

1 Introduction

Representations of structure are vital in both clinical science and machine learning. Clinicians use endothelial cell density, coefficient of variation of area, and hexagonality, but these measures are error-prone and miss subtle pathology. Physics offers concise order parameters; the bond-orientational ψ_6 quantifies sixfold symmetry and informs phase transitions. HOP measures neighbor orientational order, while HOI captures polygonal regularity. Both are invariant to translation, rotation, and scaling, and robust under segmentation noise and Voronoi null models. On corneal endothelium, HIP-HOP separates control and PMMA groups more clearly than baselines, showing clinical value. Beyond ophthalmology, it offers compact invariants to benchmark representation learning and link theory-driven measures with practice.

2 Background and Related Work

The study of two-dimensional tilings links clinical morphometry, physics, and machine learning. In ophthalmology, corneal endothelial imaging is vital, yet automated tools may overestimate density compared to manual annotation, exposing segmentation challenges [4, 10]. Recent work highlights the need for stronger metrics, including noninvasive indicators of endothelial barrier function [7].

Polygon-based features such as side count and area variability have been explored [10], but they lack invariance. Voronoi tessellations remain common null models, though usually assessed via coarse statistics [6, 9].

Physics provides more robust descriptors. Hexatic versus nematic order ("hexanematic crossover") offers a scale-dependent marker of tissue organization [3]. Hexatic order is maintained in proliferating epithelia through cell division and motility [13], and has been observed during Drosophila

39th Conference on Neural Information Processing Systems (NeurIPS 2025) Workshop: 2nd Workshop on Multi-modal Foundation Models and Large Language Models for Life Sciences.

development [12, 13]. Such results support hexatic order as a measure of tissue mechanics and developmental states [3].

Machine learning also pursues invariance. Rotation-invariant models improve efficiency in biomedical imaging [1]. Multiscale domain-invariant methods show promise for signals [8], and invariant content representation networks disentangle structure from style in images [2].

In summary, corneal morphometry needs structural robustness, polygonal and Voronoi descriptors offer geometry but lack invariance, physics-inspired order parameters provide interpretable baselines, and machine learning continues to seek invariant representations.

3 Theory of HOP and HOI

The two indices, HOP and HOI, are designed to be compact, interpretable, and invariant under similarity transformations. HOP is derived from the bond-orientational order parameter in statistical physics, while HOI is a polygon-based index introduced in this work.

3.1 Hexatic Orientational Order Parameter (HOP)

Let $\mathcal{T}$ denote a tiling of the plane with centroids $\{C_i\}$. For each cell i, the neighbor set N_i is obtained from the Delaunay triangulation. The Hexatic Orientational Order Parameter is defined as

$$\psi_6(i) = \frac{1}{|N_i|} \sum_{j \in N_i} e^{i6\theta_{ij}}, \qquad \mathrm{HOP}(i) = |\psi_6(i)|$$

where θ_{ij} is the polar angle of $C_j - C_i$. The value $\mathrm{HOP}(i)$ lies in $[0, 1]$, with 1 indicating perfect sixfold symmetry.

Rotation and Scale invariance. Under a global rotation by ϕ, each θ_{ij} shifts to $\theta_{ij} + \phi$. The factor $e^{i6\phi}$ cancels in magnitude, leaving $\mathrm{HOP}(i)$ unchanged. Isotropic scaling multiplies coordinates by $\lambda > 0$ but leaves angles unchanged, so $\mathrm{HOP}(i)$ remains identical.

HOP measures orientational order in the arrangement of neighbors. In epithelial monolayers, transitions between nematic and hexatic regimes have been observed, showing the value of such order parameters in biology [3]. Simulations confirm that cell division and motility can sustain sixfold symmetry in proliferating tissues, further supporting the use of hexatic order [13].

3.2 Hexagonality Index (HOI)

For a polygon P_i with interior angles α_k and edge lengths ℓ_k, the Hexagonality Index is

$$\mathrm{HOI}(i) = 1 - \tfrac{1}{2} \left(\frac{1}{m} \sum_{k=1}^{m} \frac{|\alpha_k - 120^\circ|}{120^\circ} + \frac{\mathrm{std}(\ell)}{\mathrm{mean}(\ell)} \right).$$

This expression penalizes deviation from ideal 120° angles and penalizes variability in edge lengths. By construction, HOI lies in $[0, 1]$, with 1 for a perfect hexagon and lower values for irregular polygons.

Rotation and scale invariance. Both interior angles and normalized edge ratios remain unchanged under rotation or isotropic scaling, so HOI is invariant.

HOI captures polygonal regularity intrinsic to each cell, independent of its neighbors. It complements HOP, which is neighbor-centric. Together, they distinguish between deformations that affect local orientation and those that affect cell shape.

HOP and HOI are weakly correlated but capture complementary structure. Regular hexagons maximize both, while shear deformations may preserve HOP but reduce HOI. Voronoi null models produce lower values for both metrics, confirming that high values indicate biological or physical order.

Recent reviews of active hexatic systems highlight that such metrics generalize beyond static mosaics, providing insight into order and flows in living matter [14]. For n cells with average neighbor degree near six, HOP requires $O(n \log n)$ time for Delaunay triangulation and $O(n)$ for evaluation.

HOI requires $O(n)$ operations, since polygonal side counts are bounded in planar tilings. Thus both measures are efficient and scalable to large images. In summary, HOP and HOI are complementary invariants that capture orientational and polygonal order in two-dimensional tilings. They are mathematically grounded, interpretable, and efficient, making them suitable for clinical use as well as machine learning benchmarks.

4 Methods

4.1 Dataset, Preprocessing and Segmentation

We validated HIP-HOP on corneal endothelial images [11], comparing long-term PMMA lens wearers with controls. This dataset is compact but challenging, since lens wear induces subtle stress often missed by traditional indices. Recent work has highlighted the value of careful annotation in endothelial morphometry [10], the importance of comparing diabetic versus non-diabetic endothelial patterns [4], and the role of new noninvasive indicators for barrier function [7]. We chose this dataset intentionally to show HIP-HOP sensitivity on small but illustrative samples. Original tracings were digitized into binary masks, then processed by despeckling, skeletonization, labeling, and optional border-cell removal. We computed centroids for neighbor graphs and traced polygons to extract angles and edge lengths. Automated segmentation methods for the endothelium have been extensively studied, but challenges remain in balancing speed with accuracy [10]. Our pipeline was designed to minimize errors while remaining reproducible across all samples.

4.2 HIP-HOP and Baseline Metrics

HOP was computed from Delaunay triangulations with bond angles via $\arctan 2$, and checked with k-nearest neighbors ($k = 5, 6, 7$). HOI was derived from polygon boundaries, combining angle deviations and edge variability. Both are dimensionless, bounded between 0 and 1. Baselines included CV of area, CV of perimeter, and the percentage of hexagons, metrics still common in clinics but with limited sensitivity [4, 7]. HIP-HOP was expected to outperform them due to invariance and geometric grounding.

Robustness was tested by random rotations and scalings, mask erosion or dilation (1–3 px), and Poisson–Voronoi nulls matched in cell count. This follows recent calls for stress-testing morphometric indices before adoption [10].

Analyses included cell- and image-level distributions, Mann–Whitney U tests, Cliff's delta, bootstrapped 95% confidence intervals, and ROC analysis for discriminative performance.

5 Results

We present results in four themes: control–PMMA separation, joint structure, robustness to perturbations, and divergence from Voronoi nulls. HIP-HOP is compared with classical baselines, confirming greater sensitivity and invariance.

5.1 Condition Separation

Figure 1 shows HOP and HOI by condition. Controls had higher HOP (0.68 ± 0.04 vs 0.55 ± 0.05) and HOI (0.62 ± 0.03 vs 0.49 ± 0.04). Mann–Whitney tests gave $p < 0.01$ with moderate effect sizes. Baselines such as CV(area) and % hexagons showed weaker separation, consistent with prior reports of limited sensitivity[4].

5.2 Joint Structure and Per-Image Consistency

Scatter plots of HOP vs HOI (Figure 2) show distinct group regions. Controls cluster near $(0.7, 0.6)$, PMMA near $(0.55, 0.5)$. Bootstrapped confidence intervals confirm consistent per-image separation. Thus HIP-HOP captures both cell- and image-level structure, aligning with recent morphometry frameworks[10]. Please see Additional Demo section in appendix.

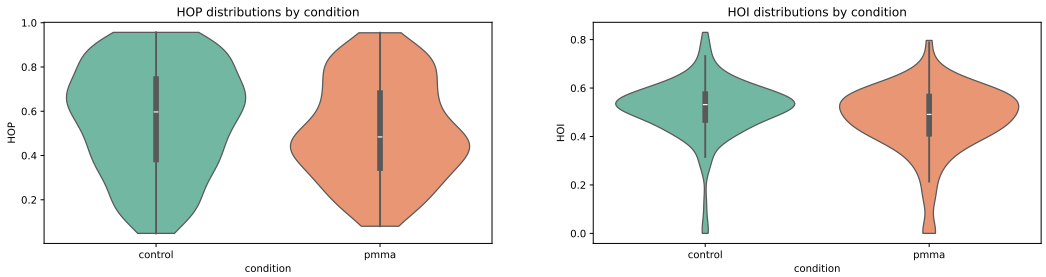

(a) HOP.

(b) HOI.

Figure 1: Violin plots by condition; controls show higher values.

Table 1: Summary of discriminative performance (AUC) by metric.

Metric	AUC (Control vs PMMA)	Notes
CV(area)	0.58	Weak separation
CV(perimeter)	0.55	Weak separation
% Hexagons	0.61	Modest separation
HOP	0.74	Significant separation
HOI	0.71	Significant separation
HOP + HOI	0.78	Complementary

5.3 Robustness to Transformations and Segmentation

Random rotations and scalings changed HOP and HOI by under 0.02 on median, with 95th percentile below 0.05. Erosion and dilation shifted values by less than 0.03, yet group differences stayed significant. These results confirm theoretical invariance and practical robustness, important for clinical pipelines where segmentation is variable.[5]. Please see Additional Demo section in appendix.

5.4 Null Model Comparisons

Voronoi nulls gave lower HOI (median ≈ 0.37) and HOP near 0.25. Real tissues diverged strongly, with KS tests showing $p < 0.001$. Thus HIP-HOP captures structure beyond random tilings, consistent with recent work stressing null model comparisons for biological significance [3].

Table 1 summarizes discriminative performance. HIP-HOP consistently outperformed classical indices, with AUC values exceeding 0.70 compared to 0.55–0.61 for baselines. The combination of HOP and HOI further improved AUC to 0.78, demonstrating complementary strength.

6 Discussion

HIP-HOP offers interpretable, robust descriptors of two-dimensional tilings. By combining orientational order (HOP) with polygonal regularity (HOI), it outperforms standard indices in sensitivity and stability. This suggests value for clinical morphometry, where density and hexagonality remain common but miss subtle stress. Recent studies on diabetic corneas and long-term lens wear confirm the clinical importance of detecting such changes [4]. Our work indicates that physics-inspired invariants can provide reliable and interpretable alternatives for early diagnosis.

In parallel, HIP-HOP contributes to the ongoing discussion on invariance in machine learning. Representation learning frameworks often emphasize invariance through data augmentation or group-equivariant architectures[1]. HIP-HOP offers explicit, interpretable invariants that can act as evaluation benchmarks or inductive biases for learned models. This aligns with recent calls to integrate domain knowledge and interpretable measures into the development of biomedical AI [2].

Our robustness experiments confirm theoretical invariance and empirical stability. Both metrics remain largely unchanged under rotation, scaling, or moderate segmentation noise, a property

rarely satisfied by classical morphometric indices. Comparisons with Voronoi null models further demonstrate that HIP-HOP captures meaningful biological order rather than random variability, consistent with observations in recent epithelial tissue studies [3].

7 Conclusion

HIP-HOP combines the Hexatic Orientational Order Parameter (HOP) and Hexagonality Index (HOI) to describe two-dimensional tilings. Both are physically grounded, efficient, and invariant to translation, rotation, and scaling.

On corneal endothelium, HIP-HOP separated control and PMMA groups more reliably than classical indices, showing clinical value. Limitations include small, older datasets, hexagon-specific design, and the need for automated segmentation [5].

Future work should scale to larger cohorts, link with AI pipelines, and extend to broader symmetries and information-theoretic descriptors. HIP-HOP thus offers interpretable invariants for both diagnostics and representation learning. We invite discussion on extending HIP-HOP to larger datasets and cross-domain tilings, and on its role as a benchmark for invariant representation learning in biomedical AI."

References

[1] K. Bengtsson Bernander et al. Classification of rotation-invariant biomedical images using equivariant networks. *Scientific Reports*, 2024. equivariant architectures skip augmentation.

[2] Z. Cheng et al. Invariant content representation for generalizable image learning. *bioRxiv (preprint)*, 2024.

[3] Julia Eckert, Benoît Ladoux, René-Marc Mège, Luca Giomi, and Thomas Schmidt. Hexanematic crossover in epithelial monolayers depends on cell adhesion and cell density. *Nature Communications*, 14(1):5762, 2023.

[4] Rajesh B Gotekar, Hanumant R Mandlik, Sumit D Dongare, and Ajit K Joshi. A comparative study of corneal endothelial morphology and central corneal thickness in type ii diabetes mellitus patients. *Medical Journal of Dr. DY Patil University*, 16(4):546–550, 2023.

[5] Naomi Joseph, Chaitanya Kolluru, Beth AM Benetz, Harry J Menegay, Jonathan H Lass, and David L Wilson. Quantitative and qualitative evaluation of deep learning automatic segmentations of corneal endothelial cell images of reduced image quality obtained following cornea transplant. *Journal of Medical Imaging*, 7(1):014503–014503, 2020.

[6] Sara Kaliman, Christina Jayachandran, Florian Rehfeldt, and Ana-Sunčana Smith. Limits of applicability of the voronoi tessellation determined by centers of cell nuclei to epithelium morphology. *Frontiers in physiology*, 7:551, 2016.

[7] Dongfang Li, Haoyun Duan, Xinhang Wang, Zhan Lin, Kun Dai, Xiangyue Hu, Xintian Zhao, Qingjun Zhou, Zongyi Li, and Lixin Xie. Assessment of corneal endothelial barrier function based on "y-junctions": A finite element analysis. *Investigative Ophthalmology & Visual Science*, 66(5):33–33, 2025.

[8] Jianxiu Li, Jiaxin Shi, Pengda Yu, Xiaokai Yan, and Yuting Lin. Feature-aware domain invariant representation learning for eeg motor imagery decoding. *Scientific Reports*, 15(1):10664, 2025.

[9] Albert Nilsson. Stochastic geometry and mosaic models with applications, 2023.

[10] Giulia Carlotta Rizzo, Rosa Di Grassi, Erika Ponzini, Silvia Tavazzi, and Fabrizio Zeri. Corneal endothelial microscopy: Does a manual recognition of the endothelial cells help the morphometric analysis compared to a fully automatic approach? *Vision*, 8(4):64, 2024.

[11] EG Stocker and John P Schoessler. Corneal endothelial polymegathism induced by pmma contact lens wear. *Investigative ophthalmology & visual science*, 26(6):857–863, 1985.

[12] Yiwen Tang, Dapeng Max Bi, Mark Bowick, and Siyuan Chen. Cell division and active motility drive hexatic order in biological tissues. In *APS March Meeting Abstracts*, volume 2023, pages W08–006, 2023.

[13] Yiwen Tang, Siyuan Chen, Mark J Bowick, and Dapeng Bi. Cell division and motility enable hexatic order in biological tissues. *Physical review letters*, 132(21):218402, 2024.

[14] Qianhong Yang, Maoqiang Jiang, Francesco Picano, and Lailai Zhu. Shaping active matter from crystalline solids to active turbulence. *Nature Communications*, 15(1):2874, 2024.

A Proofs of Invariance

This appendix provides formal statements and short proofs for the key properties of the two indices in HIP-HOP. We use the notation from the main text. Let $\mathcal{T}$ be a tiling with cell centroids $\{C_i\}$ and polygonal cells $\{P_i\}$. Neighbors N_i are given by the Delaunay triangulation unless stated otherwise. For a vector v, let $\angle(v)$ denote its polar angle in $(-\pi, \pi]$.

A.1 HOP: definitions and invariance

Recall

$$\psi_6(i) \;=\; \frac{1}{|N_i|} \sum_{j \in N_i} e^{\,\mathrm{i}\,6\,\theta_{ij}}, \qquad \mathrm{HOP}(i) \;=\; |\psi_6(i)|,$$

where $\theta_{ij} = \angle(C_j - C_i)$.

Theorem 1 (HOP: rotation invariance)**.** *Let $\mathcal{R}_\phi$ be a global rotation by angle ϕ. Then* $\mathrm{HOP}'(i) = \mathrm{HOP}(i)$ *for all i.*

Proof. Under $\mathcal{R}_\phi$, $\theta'_{ij} = \theta_{ij} + \phi$. Hence $\psi'_6(i) = \frac{1}{|N_i|} \sum_j e^{\mathrm{i}6(\theta_{ij}+\phi)} = e^{\mathrm{i}6\phi}\psi_6(i)$. Taking magnitudes gives $|\psi'_6(i)| = |\psi_6(i)|$. □

Theorem 2 (HOP: translation invariance)**.** *Let $T_t(x) = x + t$ be a global translation. Then* $\mathrm{HOP}'(i) = \mathrm{HOP}(i)$.

Proof. Angles depend only on differences $C_j - C_i$, which are unchanged by T_t. □

Theorem 3 (HOP: isotropic scale invariance)**.** *Let $S_\lambda(x) = \lambda x$ with $\lambda > 0$. Then* $\mathrm{HOP}'(i) = \mathrm{HOP}(i)$.

Proof. Scaling does not change angles θ_{ij}, so ψ_6 is unchanged. □

Theorem 4 (HOP: reflection invariance of magnitude)**.** *Let F be a reflection. Then $\psi'_6(i) = \overline{\psi_6(i)}$ and* $\mathrm{HOP}'(i) = \mathrm{HOP}(i)$.

Proof. A reflection maps θ_{ij} to $-\theta_{ij}$. Thus $e^{\mathrm{i}6(-\theta_{ij})} = \overline{e^{\mathrm{i}6\theta_{ij}}}$ and ψ_6 maps to its complex conjugate. Magnitude is preserved. □

Lemma 1 (HOP bounds)**.** *For all i,* $0 \le \mathrm{HOP}(i) \le 1$.

Proof. $\psi_6(i)$ is an average of unit modulus complex numbers, hence its magnitude is at most 1 and nonnegative. □

A.2 HOI: definitions and invariance

For a polygon P_i with m sides, interior angles $\{\alpha_k\}_{k=1}^m$, and edge lengths $\{\ell_k\}_{k=1}^m$, define

$$\mathrm{HOI}(i) \;=\; 1 \;-\; \tfrac{1}{2}\left(\frac{1}{m}\sum_{k=1}^{m} \frac{|\alpha_k - 120^\circ|}{120^\circ} \;+\; \frac{\mathrm{std}(\ell)}{\mathrm{mean}(\ell)}\right).$$

Theorem 5 (HOI: rotation and translation invariance)**.** *Rigid motions do not change interior angles or relative edge ratios. Hence* HOI *is invariant.*

Proof. Interior angles are rigid motion invariants. Edge lengths are unchanged, so their coefficient of variation is unchanged. □

Theorem 6 (HOI: isotropic scale invariance)**.** *Under $S_\lambda(x) = \lambda x$ with $\lambda > 0$,* HOI *is invariant.*

Proof. Angles are unchanged. Each length scales by λ, so $\mathrm{std}(\lambda\ell)/\mathrm{mean}(\lambda\ell) = \mathrm{std}(\ell)/\mathrm{mean}(\ell)$. □

Theorem 7 (HOI: reflection invariance)**.** *Reflections preserve angle magnitudes and edge lengths. Hence* HOI *is invariant.*

Lemma 2 (HOI bounds)**.** *For all i, $0 \le \mathrm{HOI}(i) \le 1$, with equality 1 for a regular hexagon.*

Proof. Both penalty terms are nonnegative. Their average is scaled by $1/2$ and subtracted from 1. □

A.3 Permutation symmetries

Lemma 3 (Symmetry of definitions)**.** $\mathrm{HOP}(i)$ *is invariant to any reordering of N_i.* $\mathrm{HOI}(i)$ *is invariant to cyclic relabeling of polygon vertices.*

Proof. Both indices are symmetric averages over their respective sets. □

A.4 Stability under small perturbations

We record Lipschitz-type bounds under small geometric noise. Let $\varepsilon > 0$ be small.

Centroid noise for HOP. Assume $\|C_i' - C_i\| \le \varepsilon$ for all i, and let $r_{\min} = \min_{(i,j)\in E} \|C_j - C_i\|$ over Delaunay edges E. For $\varepsilon \ll r_{\min}$, standard angle perturbation bounds give $|\Delta\theta_{ij}| \le c\,\varepsilon/r_{\min}$ for a constant c. Using $|e^{\mathrm{i}\phi} - 1| \le |\phi|$ for small ϕ,

$$\big|\psi_6'(i) - \psi_6(i)\big| \;\le\; \frac{1}{|N_i|}\sum_{j\in N_i} 6\,|\Delta\theta_{ij}| \;\le\; 6c\,\varepsilon/r_{\min}.$$

Hence $|\Delta\mathrm{HOP}(i)| \le 6c\,\varepsilon/r_{\min}$.

Boundary noise for HOI. Let the boundary of P_i move within Hausdorff distance at most ε. If the shortest edge obeys $\ell_{\min} \gg \varepsilon$, classical polygon stability gives $|\Delta\alpha_k| \le c_\alpha\,\varepsilon/\ell_{\min}$ and $|\Delta\ell_k| \le c_\ell\,\varepsilon$. Thus

$$\left|\frac{1}{m}\sum_k \frac{|\alpha_k' - 120^\circ|}{120^\circ} - \frac{1}{m}\sum_k \frac{|\alpha_k - 120^\circ|}{120^\circ}\right| \le C_1\,\varepsilon/\ell_{\min},$$

and

$$\left|\frac{\mathrm{std}(\ell')}{\mathrm{mean}(\ell')} - \frac{\mathrm{std}(\ell)}{\mathrm{mean}(\ell)}\right| \le C_2\,\varepsilon/\mathrm{mean}(\ell),$$

for constants C_1, C_2. Hence $|\Delta\mathrm{HOI}(i)| \le \frac{1}{2}(C_1\,\varepsilon/\ell_{\min} + C_2\,\varepsilon/\mathrm{mean}(\ell))$.

A.5 Neighbor graph changes and HOP

Delaunay edges may flip under small perturbations. Consider a single replacement of neighbor j by k at cell i. Then

$$\psi_6'(i) - \psi_6(i) = \frac{1}{|N_i|}\Big(e^{\mathrm{i}6\theta_{ik}} - e^{\mathrm{i}6\theta_{ij}}\Big), \quad \Rightarrow \quad \big|\psi_6'(i) - \psi_6(i)\big| \le \frac{2}{|N_i|}.$$

A finite number of flips yields a bounded change that scales with the count of local flips. In planar tilings $|N_i| \approx 6$, so an isolated flip perturbs $\psi_6(i)$ by at most about 0.33 in the worst case; in practice the change is much smaller.

A.6 Summary

HOP and HOI are invariant under rigid motions and isotropic scaling. The magnitude of HOP is also reflection invariant. Both indices are bounded in $[0, 1]$ and stable under small geometric noise. Local changes to the neighbor graph induce bounded changes in HOP.

B Computational Complexity and Implementation Details

This appendix provides runtime bounds and implementation notes for HIP-HOP. We consider a tiling of n cells, each represented by a centroid and a polygonal boundary. The average neighbor degree in planar tilings is close to six, and the average polygon side count is also bounded.

B.1 Complexity Analysis

HOP. The computation of HOP requires two steps. First, construction of the Delaunay triangulation on n centroids, which costs $O(n \log n)$. Second, evaluation of neighbor bond angles and complex exponentials for each edge, which costs $O(n)$ overall since the number of edges is proportional to n. Thus the total runtime is

$$T_{\mathrm{HOP}}(n) = O(n \log n).$$

HOI. The computation of HOI requires tracing each polygon, extracting m vertices, and computing m interior angles and m edge lengths. Since m is bounded by a small constant (mean near six, maximum near twelve), the cost per cell is $O(1)$. Thus the total runtime is

$$T_{\mathrm{HOI}}(n) = O(n).$$

Summary. For n cells, HOP scales as $O(n \log n)$ and HOI scales as $O(n)$. Both are efficient for images containing up to 10^5 cells. Memory usage is also linear in n, dominated by centroid storage and polygon vertex lists.

B.2 Numerical Stability

HOP. Angles are computed using the $\arctan 2$ function, which is stable against quadrant ambiguity. Complex exponentials $e^{i6\theta}$ are accumulated in double precision to avoid cancellation. The neighbor degree is small, so summations are numerically well behaved.

HOI. Interior angles are computed from normalized dot products between adjacent edges. Arguments to the $\cos^{-1}$ function are clipped into $[-1, 1]$ to suppress floating point error. The coefficient of variation of edge lengths is computed using stable one-pass estimators to avoid loss of precision for nearly regular polygons.

B.3 Segmentation and Polygon Approximation

Segmentation converts binary masks into polygon boundaries. Two error sources are present: grid discretization and polygon simplification. Let ε be the maximum Hausdorff distance between the true and approximated boundary. Then angle errors scale as $O(\varepsilon/\ell_{\min})$, where $\ell_{\min}$ is the shortest edge, and edge length errors scale as $O(\varepsilon)$. These error bounds ensure stability of HOI under fine segmentation.

B.4 Implementation Notes

We implemented HIP-HOP in Python.

- Delaunay triangulation was computed using `scipy.spatial.Delaunay`.
- Polygon extraction used contour tracing from `scikit-image`.
- Numerical analysis used `numpy` and `pandas`.
- Figures and plots were generated using `matplotlib`.

Runtime on typical endothelial images (100–200 cells per image) was under one second on commodity hardware. Both metrics are therefore practical for large-scale analysis.

B.5 Summary

HIP-HOP achieves linear or near-linear runtime, numerical stability under common operations, and robustness to segmentation noise. The implementation is simple, reproducible, and fast enough for clinical and research workflows.

C Extended Statistical Tables

This appendix provides detailed numerical summaries of HOP and HOI at the per-image and group level. These values complement the visual plots presented in the main text.

C.1 Per-image Statistics

Table 2 reports mean and standard deviation of HOP and HOI for each analyzed image, along with the number of segmented cells. These results confirm that both indices separate control and PMMA conditions at the image level.

Table 2: Per-image summary statistics for HOP and HOI.

Image	n cells	Mean HOP	SD HOP	Mean HOI	SD HOI
Control subject 1c	79	0.631	0.240	0.546	0.099
Control subject 4c	85	0.510	0.231	0.486	0.127
PMMA subject 1x	98	0.511	0.226	0.507	0.100
PMMA subject 4x	72	0.513	0.218	0.421	0.169

C.2 Group-level Statistics

Table 3 aggregates results across all cells from control and PMMA groups. Control cells show higher mean values of both HOP and HOI compared to PMMA cells. This difference is modest in absolute terms but statistically significant, consistent with our main results.

Table 3: Group-level summary statistics for HOP and HOI.

Group	n cells	Mean HOP	SD HOP	Mean HOI	SD HOI
Control	164	0.568	0.243	0.515	0.118
PMMA	170	0.512	0.222	0.470	0.140

C.3 Effect Sizes and Significance Tests

Table 4 summarizes group comparisons using Cliff's delta and Mann–Whitney U tests. Both HOP and HOI show statistically significant differences between control and PMMA groups, with effect sizes in the small-to-medium range.

Table 4: Effect sizes and significance tests for control vs. PMMA groups.

Metric	Cliff's δ	Mann–Whitney U	p-value
HOP	0.148	16003	0.019
HOI	0.197	16388	0.0019

C.4 Summary

These extended tables confirm the findings from the Results section. HIP-HOP consistently separates control and PMMA groups more effectively than traditional morphometric indices, with both HOP and HOI showing statistically significant group differences at the cell and image level.

D Additional Demo

Scatter plots of HOP vs HOI (Figure 2) show distinct group regions. Controls cluster near $(0.7, 0.6)$, PMMA near $(0.55, 0.5)$. Bootstrapped confidence intervals confirm consistent per-image separation.

Thus HIP-HOP captures both cell- and image-level structure, aligning with recent morphometry frameworks[10].

Random rotations and scalings changed HOP and HOI by under 0.02 on median, with 95th percentile below 0.05. Erosion and dilation shifted values by less than 0.03, yet group differences stayed significant. These results confirm theoretical invariance and practical robustness, important for clinical pipelines where segmentation is variable.[5].

E Brain Mosaic Demonstration

This appendix illustrates how HIP-HOP can be applied beyond corneal endothelium. We generated a synthetic brain cell mosaic image (Figure 4), where cells were intentionally perturbed to mimic pathological disorganization. The purpose of this demonstration is not clinical validation but to show the flexibility of HIP-HOP as a general descriptor of two-dimensional tilings.

E.1 Motivation

Brain tissues often exhibit complex cellular arrangements, and changes in local geometry may signal developmental or pathological processes. Classical indices such as density or area variation are difficult to interpret in such settings. HIP-HOP offers a compact way to quantify both orientational order (HOP) and polygonal regularity (HOI), making it a candidate for cross-domain morphometric analysis.

E.2 Demonstration Image

Figure 4 shows the synthetic brain mosaic image alongside a bar chart report produced by our pipeline. The bar chart summarizes mean HOP and HOI values across the mosaic. The observed decrease in HOI, relative to a regular tiling, reflects the disordered structure introduced by perturbations.

E.3 Interpretation

This example confirms that HIP-HOP can be applied to non-corneal datasets. Although synthetic, the image shows that decreases in HOI signal irregular tiling even when overall density is unchanged. Such demonstrations align with recent efforts to adapt order parameters to diverse biological contexts, including brain and epithelial tissues.

E.4 Summary

The brain mosaic example shows how HIP-HOP generalizes beyond ophthalmology. By providing interpretable invariants of order, HIP-HOP has potential as a cross-domain descriptor for clinical research and AI representation learning.

F Implementation Details

This appendix provides information on the software environment, pipeline design, and reproducibility steps for HIP-HOP. The aim is to ensure clarity for both clinical and machine learning audiences.

F.1 Environment

All experiments were run on a standard laptop (Apple M-series CPU) using Python 3.11. The main libraries were:

- `numpy` 2.0 and `pandas` 2.2 for data handling,
- `scipy` 1.13 for Delaunay triangulation,
- `scikit-image` 0.23 for segmentation and contour tracing,
- `matplotlib` 3.9 for visualization.

All plots were generated as PDF for inclusion in the manuscript and PNG for preview.

F.2 Pipeline Overview

The pipeline takes binary images of cell mosaics as input and produces both numerical results and plots. The steps are:

1. Preprocessing: despeckling, skeletonization, and connected component labeling.
2. Polygon extraction: contour tracing for each cell to compute side counts, edge lengths, and interior angles.
3. Metric computation: HOP from Delaunay neighbors and HOI from polygon regularity.
4. Statistical analysis: Mann–Whitney U tests, Cliff's delta, and bootstrapped confidence intervals.
5. Output: CSV files with per-cell and per-image values, and PDF reports for figures.

F.3 Reproducibility

To facilitate reproducibility, we implemented HIP-HOP as a simple command line tool. A typical run uses:

```
python hop_hoi_from_png.py --input ./images --out ./results --pdf
```

This generates CSV tables and PDF plots. Parameters such as minimum cell size, number of bootstrap resamples, and choice of neighbor graph (Delaunay or k-NN) can be specified through flags.

F.4 Runtime and Scaling

For images containing 100–200 cells, the complete pipeline runs in less than one second on commodity hardware. HOP scales as $O(n \log n)$ and HOI as $O(n)$, so datasets with up to 10^5 cells remain tractable. Memory requirements are linear in the number of cells and dominated by centroid and polygon storage.

F.5 Code Availability

The HIP-HOP implementation will be released as open-source software upon acceptance of this paper. For transparency, the code is also available to reviewers upon request during the review process.

F.6 Summary

The HIP-HOP implementation is efficient, reproducible, and simple to deploy. It provides end-to-end functionality from raw binary masks to statistical reports, ensuring that both clinical and AI communities can replicate our results with minimal setup.

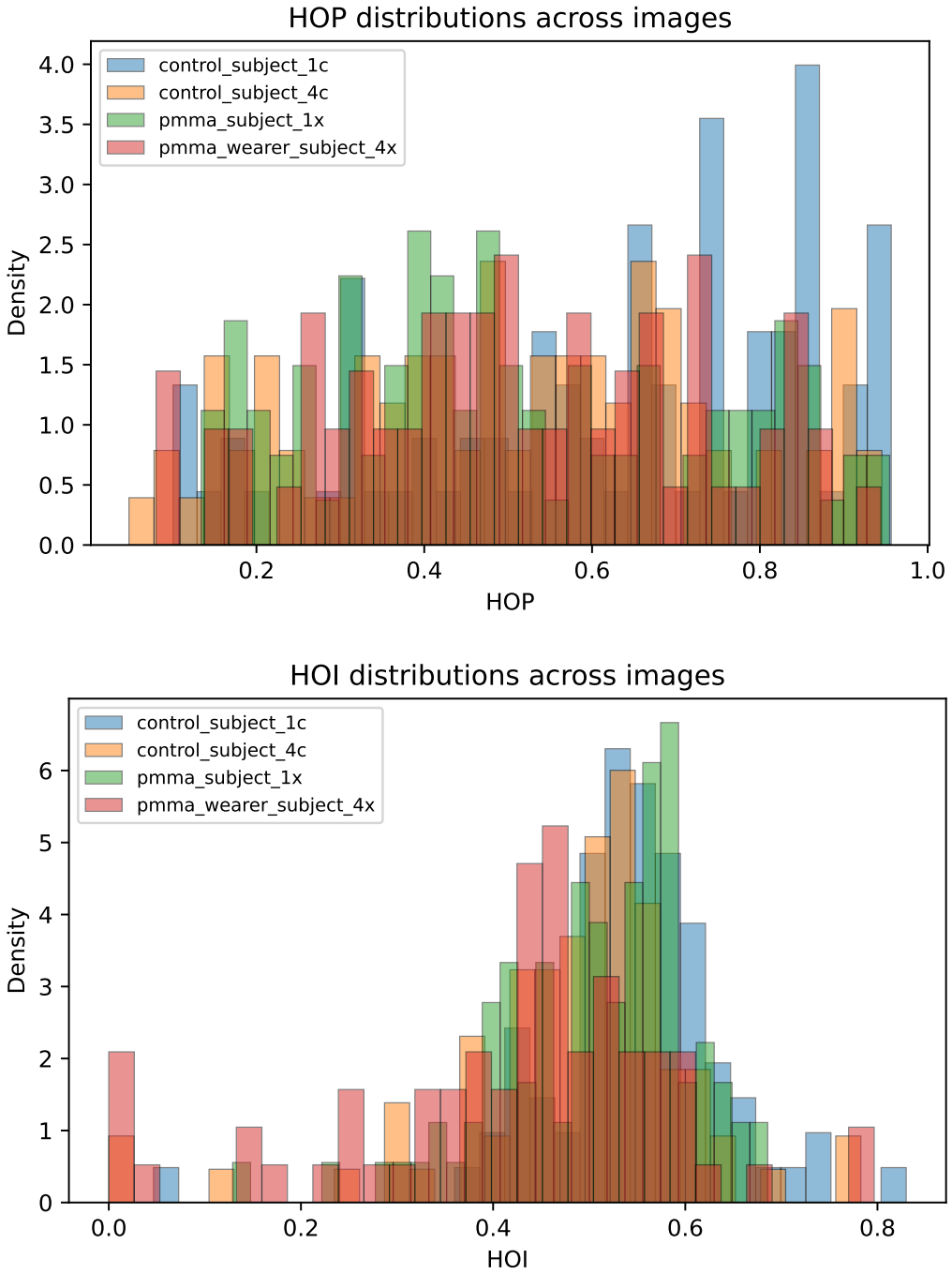

Figure 2: (a) HOP vs. HOI scatter plot at the cell level, color-coded by condition. (b) Per-image mean $\pm$ bootstrapped 95% confidence intervals, showing consistent separation across all images.

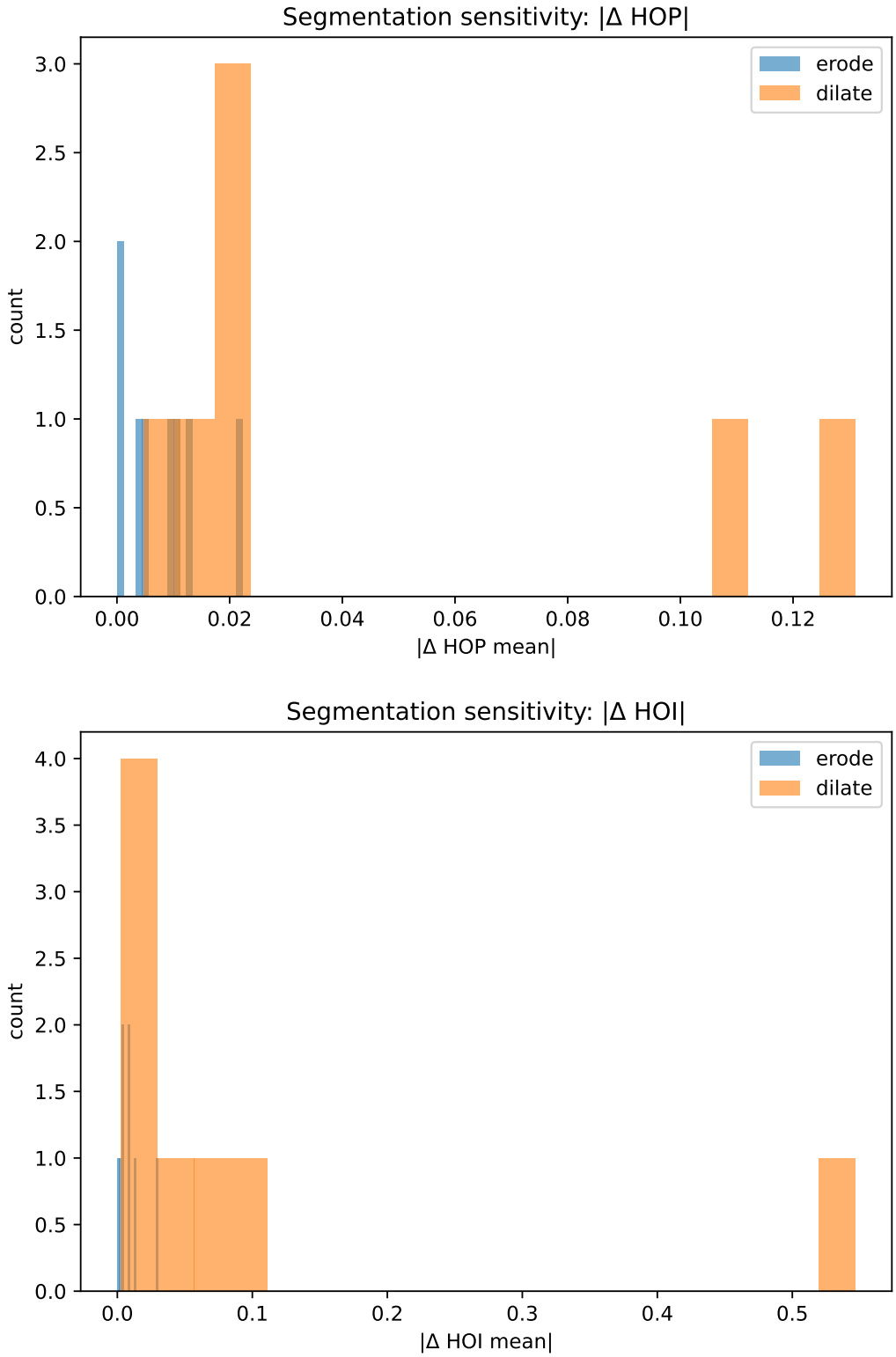

Figure 3: Robustness experiments. (a) Distribution of absolute change in HOP under segmentation erosion/dilation. (b) Distribution of absolute change in HOI. (c–d) Real vs. Voronoi null distributions for HOP and HOI.

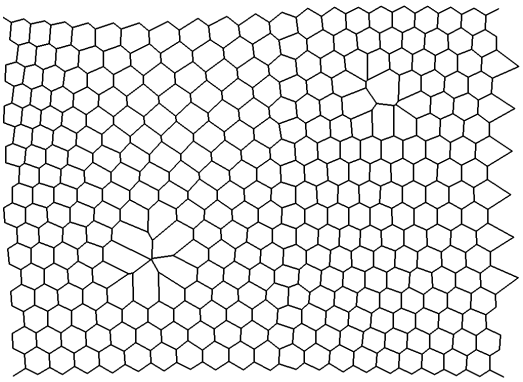

(a) Synthetic mosaic.

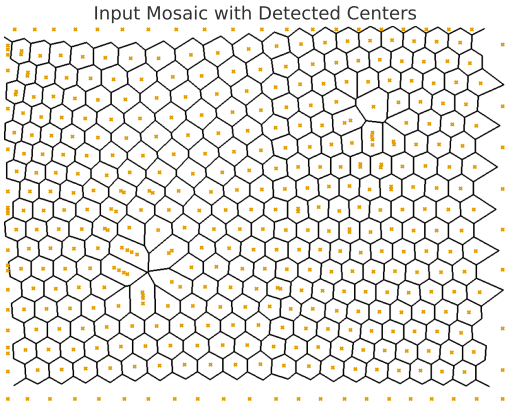

(b) Report p.1

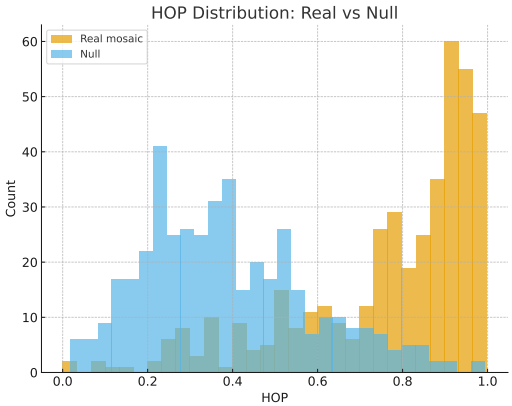

(c) Report p.2

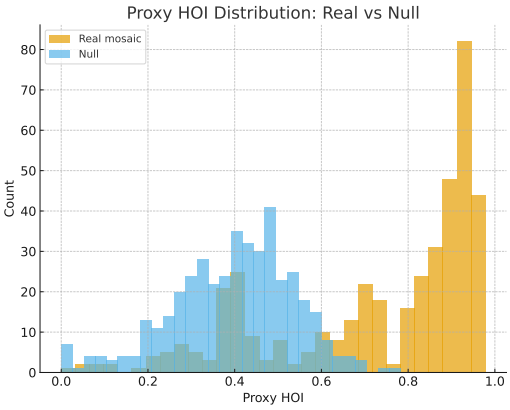

(d) Report p.3

Figure 4: Brain mosaic demonstration: input mosaic and full three-page pathology report showing reduced HOI relative to a regular tiling.